Journal of the European Ceramic Society **17** (1997) 1099–1112

PII: S0955-2219(96)00218-X
0955-2219/97/$17.00

Microstructural Stability of Duplex α–β-Sialon Ceramics

Lena K. L. Falk,[a,*] Zhi-Jian Shen[b] and Thommy Ekström[c]

[a]Department of Physics, Chalmers University of Technology, S-412 96 Göteborg, Sweden
[b]Department of Materials Science & Engineering, Zhejiang University, Hangzhou 310027, People's Republic of China
[c]Department of Inorganic Chemistry, Arrhenius Laboratory, University of Stockholm, S-106 91 Stockholm, Sweden

(Received 8 August 1996; accepted 21 October 1996)

Abstract

Duplex Y-, Yb- and Nd-doped α–β-sialon ceramics were fabricated from starting powder compositions within the two-phase α′–β′ area. The microstructures contained high aspect ratio β-sialon grains homogeneously distributed in an α-sialon matrix and only smaller volume fractions of intergranular phases. The morphology of the intergranular regions was determined by the overall chemistry and the doping element. The β′/α′+β′ weight ratio as well as the α and β-sialon substitution levels were dependent upon the α′ stabilizing cation. Sialons with an β′/α′+β′ weight ratio of around 0·5 had a favourable combination of high hardness, HV_{10} around 21 GPa, and indentation fracture toughness, 5·0–5·5 MPa $m^{1/2}$. The toughness of these duplex sialons was however reduced to below 4 MPa $m^{1/2}$ after long-term heat treatment at 1450°C. The α′ stabilizing elements Y and Yb resulted in α-sialon structures which were stable during heat treatment at 1450°C, while the Nd α′ structures decomposed into Al-substituted melilite, $Nd_2Si_2AlO_4N_3$, β-sialon and the 21R sialon polytype at this temperature. The results imply that duplex α–β-sialons stabilized by Y and Yb have a high potential as engineering ceramics. © *1997 Elsevier Science Limited.*

1 Introduction

Ceramics based on Si_3N_4 have a high potential for structural applications at both low and high temperatures due to their inherently good mechanical, chemical and thermal properties. Fabrication of dense materials requires a sintering additive which, in general, is a metal oxide. The sintering process is also promoted by the addition of Al_2O_3/AlN together with a metal oxide. This combination of additives lowers the eutectic temperature of the system and thereby the required sintering temperature. β-sialon (β′), $Si_{6-z}Al_zO_zN_{8-z}$, generally forms when Al_2O_3 and AlN are added, and β-sialon ceramics are easily pressureless sintered at 1700–1750°C with additions of yttria or rare earth element oxides.[1–3] These additives promote growth of elongated β-crystals which results in a high fracture toughness. The hardness (HV_{10}) of the resulting β-sialon ceramic is, however, moderate, around 14–15 GPa. The inherent hardness of β-Si_3N_4 (around 17 GPa) is not reached because of the presence of a significant volume fraction of intergranular crystalline and/or amorphous phases in the microstructure.[3,4]

The α-sialon ceramics, on the other hand, show excellent hardness (around 22 GPa) and have attracted attention also because they offer a possibility of reducing the amount of residual glass.[5] α-sialon (α′) has an overall composition $R_xSi_{12-(m+n)}Al_{m+n}O_nN_{16-n}$; α-sialon is not only adapting Al–O (as the β-sialon), but also incorporates the R metal ion into its structure.[6–9] The interstitial sites in the α-Si_3N_4 structure set an upper limit to the radius of the R ion; cations larger than 0·1 nm (e.g. Ce^{3+}, La^{3+}) are not accepted, whereas Y and rare earth elements Yb–Nd with ionic radii in the range 0·087–0·099 nm are known to stabilize the α′-structure.

α-Sialon may be retained to room temperature by quenching from temperatures in the range 1750–1800°C. The long-term stability at intermediate temperatures of some of the α-sialons has, however, come into doubt. A slower cooling rate, as well as a post-densification heat treatment at temperatures between 1300 and 1600°C, results in a transformation of α- to β-sialon.[10,11] This process is reversible; the α′-phase is again formed when re-heating to high temperatures.[10] Studies have

*To whom correspondence should be addressed.

recently been done on the stability of pure α-sialons doped with Sm, Nd, Yb and Dy.[12–20] The smaller rare earth cations like Yb^{3+} and Dy^{3+} result in an α-sialon phase which appears stable at all temperatures and for long periods of time. α-Sialon stabilized at high temperatures by the larger rare earth cations Sm^{3+} and Nd^{3+} were found to decompose at temperatures below 1650°C. The mechanisms behind this process are still not fully understood. One contributing factor may be that these larger rare earth cations tend to form very stable Al-substituted melilite phases, $R_2Si_{3-x}Al_xO_{3+x}N_{4-x}$, (called R-M′ below) at temperatures around 1400–1500°C, and, when heat treated at slightly higher temperatures, 1500–1650°C, a new phase, JEM, $RAl(Si_{6-z}Al_z)(N_{10-z}O_z)$ forms.[15,21]

The α-sialon has a two-dimensional solid solution range in the Si_3N_4–Al_2O_3·AlN–RN·3AlN plane in the Jänecke prism describing the particular R–Si–Al–O–N system. This plane intersects the basal plane of the prism along the β-sialon solid solution line (following the Si_3N_4–Al_2O_3·AlN join) and the α-sialon is separated from the β-sialon by an α'-β' two-phase area, see Fig. 1.

It has been shown that compositions along the tie line β-Si_3N_4–R_2O_3·9AlN, which passes through the two-phase β–β'/α-sialon area, give a possibility to adjust toughness and hardness of the so-formed duplex α–β-sialon ceramic.[22–24] In-situ reinforced Y-doped α–β-sialon ceramics with a β-phase content of around 60% had a fracture toughness of 6 MPa $m^{1/2}$ and a flexural strength of 1100 and 800 MPa at 25 and 1400°C, respectively.[23]

The two-phase α–β-sialon field is thus of great interest, particularly since Y and rare earth elements promote growth of elongated, high aspect ratio β-sialon crystals. Duplex α–β ceramics may thus be designed to have a microstructure consisting of well-distributed β'-crystals in an α-sialon matrix. Carefully adjusted overall compositions would also result in a minimum volume fraction of intergranular phases.[24]

This paper describes preparation and properties of duplex α–β-sialon ceramics. Materials formed in the α'/β' area in the Y–Si–Al–O–N system are compared with duplex sialons formed in two R–Si–Al–O–N systems, where R = Yb and Nd. These R elements were chosen because they represent the size end members of rare earth cations known to stabilize the α'-phase. The long-term high-temperature stability of the different duplex α–β-sialon ceramics was of special interest since this might limit their use as structural ceramics at elevated temperatures. Phase and microstructural development and the volume fraction

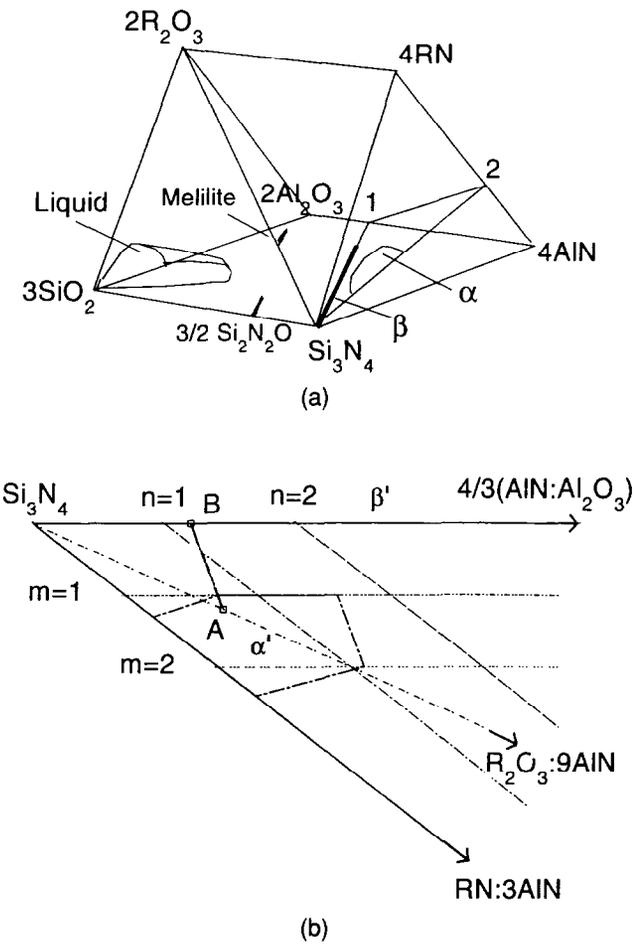

Fig. 1. A schematic illustration (a) of the Jänecke prism of an R–Si–Al–O–N system and (b) the plane containing the α- and β-sialon solid solutions. This plane has the corners Si_3N_4, 1 = AlN·Al_2O_3 and 2 = RN·3AlN. The Si_3N_4–Y_2O_3·9AlN compositional line in (b) passes the α-sialon area where point A represents the α-sialon composition aimed at by the starting powder mixtures. The compositions of the prepared starting powder mixtures fall along the line A–B.

and chemistry of residual intergranular phases were characterized and related to mechanical properties.

2 Experimental

2.1 Sialon ceramics

The overall compositions of the prepared starting powder mixtures corresponded to single-phase α-sialon and duplex α–β-sialon ceramics with different β'/α'+β' weight ratios. The composition of the α-sialon phase (A in Fig. 1(b)) was equivalent to $R_{0.4}Si_{10.2}Al_{1.8}O_{0.6}N_{15.4}$, where R = Y, Yb and Nd. The β-sialon phase was equivalent to the composition $Si_{5.4}Al_{0.6}O_{0.6}N_{7.4}$ (B in Fig. 1(b)). Powder mixtures with β/α+β-sialon weight ratios of 0, 0·3, 0·5 and 0·7 were prepared, see Table 1. These overall compositions fall along the line A–B indicated in Fig. 1(b), and would thus result in sialon ceramics with a minimum volume fraction

of intergranular phases if complete reaction takes place during densification.

Starting powder mixtures were prepared with corrections for the small amounts of oxygen present in the Si_3N_4 (Ube, SN–E10) and AlN (H. C. Starck, Berlin, grade A) raw materials corresponding to 2·7 wt% SiO_2 and 1·9 wt% Al_2O_3, respectively. The metal oxide starting powders, Al_2O_3 (Alcoa, grade A16SG), Y_2O_3 (H. C. Starck, Berlin, grade Finest) and R_2O_3 (99·9%, Johnson Matthey Chemicals Ltd), were calcined at 1000°C for 2 h before use. The powder mixtures were milled in water-free propanol for 24 h in a plastic jar using sialon milling media. Pellets of dried powders, compacted in a steel die, were hot-pressed in BN-coated graphite dies under protective nitrogen atmosphere in a graphite resistance furnace at 1800°C (32 MPa pressure, holding time 2 h). The cooling rate from the densification temperature was 50°C min^{-1}. The density of the sintered specimens was measured by Archimedes' principle.

2.2 Heat treatment

The α-sialon ceramics were heat treated at 1300, 1450, 1550, 1650 and 1750°C for 24 h. These heat treatments were carried out in order to establish the structural stability of the Y-, Yb- and Nd-doped α-sialon phases at different temperatures, and to identify the temperature where a possible 'decomposition' would be most pronounced. Long-term stability tests of the α–β-sialon ceramics with an α' to β' ratio of around 1:1 were carried out at 1450°C for 1, 10 and 30 days. The duplex sialons were first held at 1750°C for 30 min in order to equilibrate and then quenched to the final heat treatment temperature at a rate of about 400°C min^{-1}. The samples were subsequently quenched to room temperature after heat treatment. All heat treatments were carried out with the specimens embedded in a powder mixture of Si_3N_4, AlN and BN in a carbon crucible placed in a graphite furnace with nitrogen atmosphere.

2.3 Characterization

The phase compositions and substitution levels after sintering and heat treatment were determined by X-ray powder diffractometry (XRD) using a Guinier-Hägg focusing camera as described in Refs 15, 16 and 25–27. The integrated intensities of the following reflections were used in estimating the relative crystalline phase contents: (102) and (210) of the α-sialon, (101) and (210) of the β-sialon and (211) of the R-M′ phase. The presence of the 21R polytype was indicated by reflections at 2·69 Å (equivalent to the (00$\underline{21}$) spacing) and 2·64 Å (equivalent to the (101) spacing) in the X-ray diffractogram.

Hardness (HV_{10}) and indentation fracture toughness (K_{IC}) at room temperature were determined in a Vickers diamond indenter with a 98 N (10 kg) load. The fracture toughness was evaluated according to the method of Anstis *et al.* using a constant value of 300 GPa for Young's modulus.[28]

The general microstructures were characterized by scanning electron microscopy (SEM) (JEOL JSM 820 equipped with a Link AN 10 000 EDX system) of polished surfaces using back scattered electrons for imaging. The microstructures of the duplex Nd- and Yb-stabilized sialons fabricated from starting powder compositions corresponding to an $\beta'/\alpha' + \beta'$ weight ratio of 0·5 were characterized in detail by analytical transmission electron microscopy (TEM) (Philips CM200 SuperTwin FEG equipped with a Link ISIS EDX system). The fine-scale microstructure of this duplex Yb-stabilized sialon was characterized also after heat treatment at 1450°C. The SEM and TEM samples were coated with a thin evaporated carbon film in order to avoid charging under the electron beam.

3 Results and Discussion

3.1 Phase analysis

3.1.1 As-sintered sialon ceramics

Phase compositions and unit cell dimensions after hot-pressing are given in Table 1. The Y- and Yb-doped α-sialons showed reflections from α' only, whereas the Nd-doped α-sialon also contained a minor amount of Nd-melilite, see Table 1. All duplex α–β-sialon ceramics, including the Nd-stabilized microstructures, did not contain any secondary crystalline phases according to XRD. However, there were significant deviations from the $\beta'/\alpha' + \beta'$ weight ratios aimed at by the starting powder compositions, particularly at the higher β' contents, see Table 1 and Fig. 2. The results show that the $\beta'/\alpha' + \beta'$ ratios as well as the x and z values of the duplex sialons were dependent upon the α' stabilizing cation, see diagrams in Figs 2 and 3.

The unit cell dimensions of the α-phase in the duplex Yb- and Nd-stabilized sialons were shifted towards smaller values. This implies chemical compositions corresponding to lower x values than in the α-sialon materials, see Table 1 and Fig. 3. The α' phases in the Nd-stabilized sialons had the lowest x values despite the significantly reduced α' content in these materials, see Figs 2 and 3. The Yb-stabilized duplex sialons had the highest α' contents, and the Yb-doped α-sialon structures did also have the highest x values. This

Table 1. Phase compositions, measured densities and observed lattice parameters after densification of the different starting powder compositions

Starting powder	*Phase composition* α′	β′	M′	α-*sialon* a_α (*nm*)	c_α (*nm*)	β-*sialon* a_β (*nm*)	c_β (*nm*)	*Measured density* (*g cm* ^{3})
Y $\beta'/\alpha'+\beta'$:								
0	100	/	/	0·7801	0·5681	/	/	3·285
0·3	82	18	/	0·7797	0·5678	0·7620	0·2921	3·265
0·5	52	48	/	0·7801	0·5681	0·7622	0·2922	3·219
0·7	18	82	/	0·7799	0·5682	0·7621	0·2921	3·220
Yb $\beta'/\alpha'+\beta'$:								
0	100	/	/	0·7803	0·5682	/	/	3·462
0·3	87	13	/	0·7798	0·5676	0·7623	0·2923	3·393
0·5	57	43	/	0·7799	0·5678	0·7624	0·2924	3·372
0·7	20	80	/	0·7800	0·5682	0·7623	0·2922	3·251
Nd $\beta'/\alpha'+\beta'$:								
0	96	/	4	0·7806	0·5682	/	/	3·376
0·3	62	38	/	0·7801	0·5676	0·7620	0·2918	3·325
0·5	38	62	/	0·7797	0·5674	0·7618	0·2918	3·274
0·7	8	92	/	0·7795	0·5676	0·7620	0·2919	3·240

indicates that the duplex sialons formed with Nd_2O_3 had either a larger volume fraction of intergranular glass containing the α' stabilizing cation, or that the cation concentration in the intergranular regions was significantly higher than in the Yb-doped sialons. The x value of Y-doped α' did not change in any significant way when β-sialon was incorporated into the microstructure. However, the reduction in α-sialon content during densification of the starting powder mixture with a composition corresponding to an $\beta'/\alpha'+\beta'$ ratio of 0·7 indicates that this material had an increased volume fraction of an Y-rich intergranular glass, see Fig. 2.

The local substitution levels of the α' and β' phases in the Nd and Yb duplex sialons formed from starting powder compositions corresponding to an $\beta/\alpha+\beta$-sialon weight ratio of 0·5 were determined by fine probe EDX analysis in the FEGTEM. These measurements showed that there was a significant spread in the x values of the two α' phases. The Nd-stabilized α'-structure showed substitution levels ranging from $x = 0{\cdot}23$ up to $x = 0{\cdot}45$. The solid solution range of the Yb-stabilized α'-structure was shifted to smaller x values; substitution levels in the range $x = 0{\cdot}13$ to $x = 0{\cdot}35$ were measured. These x values deviate significantly from the values determined by XRD. It should, however, be pointed out that the XRD measurements give mean values for a certain volume in the microstructure and that microanalysis in the TEM will show fine-scale local equilibria in the system.

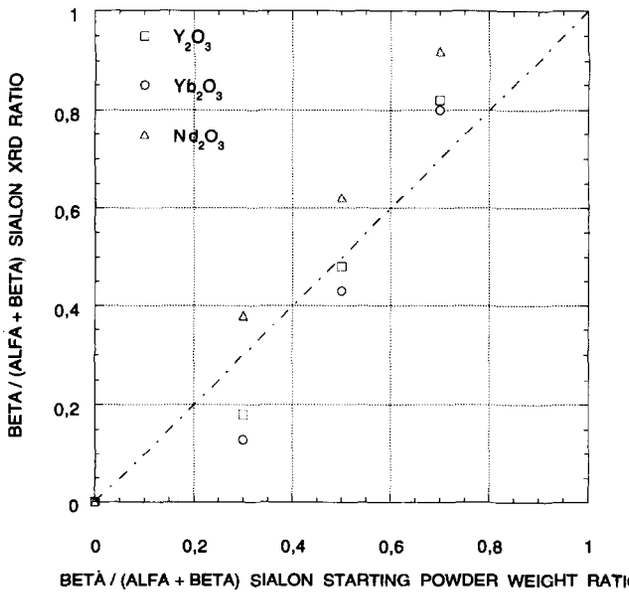

Fig. 2. $\beta/\alpha+\beta$-Sialon ratios of the duplex sialons determined by XRD as function of the $\beta'/\alpha'+\beta'$ weight ratio of the starting powder mixture and the stabilizing oxide.

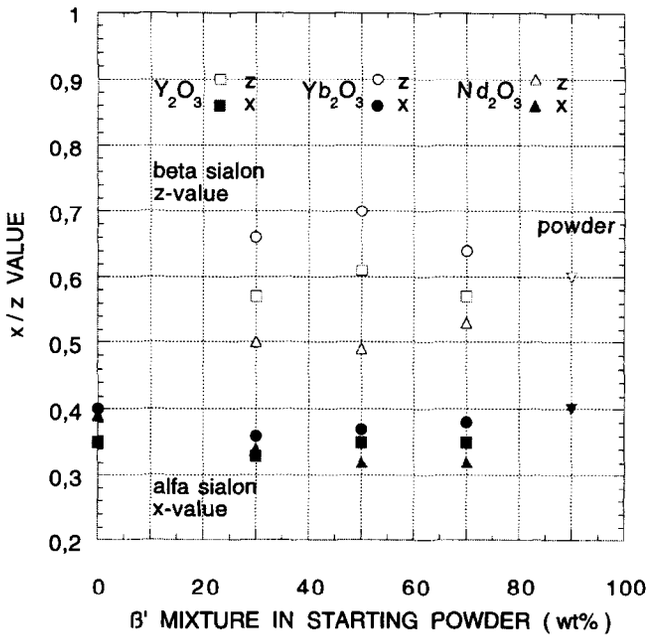

Fig. 3. α-Sialon x values and β-sialon z values in α and duplex α–β-sialons determined by XRD.

The z values of the β' phase in the duplex sialons determined by XRD also deviated from the attempted 0·60. Nd_2O_3 resulted in the lowest z values, around 0·5, while Yb_2O_3 resulted in z values larger than 0·60. The lower z values of the β'-phase in the duplex sialons formed with Nd_2O_3 would be in accordance with the significantly increased β' contents in these materials, see Figs 2 and 3. Yb_2O_3 resulted in a lower β' content except when the $\beta/\alpha+\beta$-sialon weight ratio aimed at by the starting powder mixture was increased to 0·7. This behaviour is also in good agreement with the observed z values. However, the local z values determined by EDX in the FEGTEM showed almost the same spread in β' substitution level in the Nd- and Yb-stabilized duplex sialons formed from starting powder compositions corresponding to an $\beta'/\alpha'+\beta'$ weight ratio of 0·5.z. Values in the range 0·36 to 0·79 and 0·35 to 0·72 were measured in the Nd- and Yb-stabilized materials, respectively.

XRD indicated that the lowest mean substitution level in the α-sialon ceramics was obtained by stabilization with Y, see Fig. 3. This was also the case when the $\beta'/\alpha'+\beta'$ weight ratio of the starting powder composition was 0·3. The phase compositions and substitution levels of the Y-stabilized duplex sialons were, however, in between the values obtained with the Nd- and Yb-stabilization when the β' content was increased, see Figs 2 and 3.

Thus, the results imply that the duplex sialon starting powder compositions result in equilibrium phase compositions consisting of α', β' and a residual glassy phase. The Yb-stabilized duplex sialon formed from a starting powder composition corresponding to a $\beta'/\alpha'+\beta'$ weight ratio of 0·5 did also contain smaller amounts of a secondary crystalline phase as discussed in Section 3.2.1. below. The results show that the α' and β' substitution levels and the equilibrium composition and volume fraction of the glass are dependent upon the starting powder composition as well as the α' stabilizing cation. However, more fine-scale analytical work is required in order to establish local substitution levels and phase equilibria in these sialon systems.

3.1.2 Heat treated sialon ceramics

Heat treatment of the Y-stabilized α-sialon material at temperatures in the range 1300–1750°C did not have any obvious effect on phase composition and substitution level.

The most critical temperature for heat treatment of the Yb- and Nd-stabilized α-sialon materials seemed to be at around 1450°C, where the Nd-M′ phase, $Nd_2Si_{3-x}AlxO_{3+x}N_{4-x}$, and trace amounts of Yb-garnet, $Yb_3Al_5O_{12}$, formed, see Fig. 4. The formation of these phases was accompanied by a reduction in the α' content and the formation of β'. Traces of Nd-M′ were observed after heat treatment at 1550°C, while the phase contents of the Yb-doped α-sialon appeared unaffected.

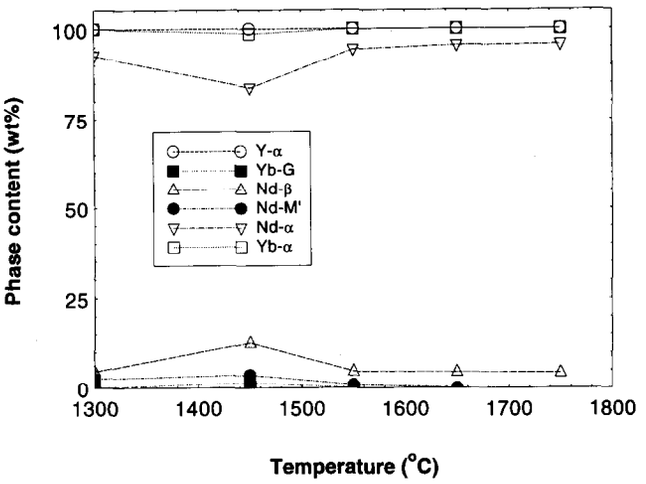

Fig. 4. The phase contents of the Y-, Yb- and Nd-doped α-sialon ceramics after heat treatment at different temperatures for one day (24 h). Note the increased formation of melilite and garnet phases at around 1450°C.

The Nd-M′ and Yb-garnet did not form during heat treatment at 1300°C. This temperature is below the eutectic temperatures of these systems which implies that the presence of a liquid phase is an aid in the decomposition of the α-sialon by providing an effective diffusion path. It also appears that the driving force for decomposition is largest at around 1450°C. A similar type of behaviour has been demonstrated by Mandal *et al.*;[10] heat-treatment at 1450°C resulted in extensive phase changes in a number of rare-earth-doped α-β-sialons.

The phase contents of the heat-treated Y-doped α–β-sialon after different times at 1450°C is shown in Fig. 5(a). The results show a slowly decreasing α' content and a simultaneously increasing β' content with time at temperature. Some Y-M′ formed during the first 10 days, but the amount did not increase with a prolonged heat treatment time. This might be interpreted as the early devitrification of residual liquid phase to Y-M′. This process may also require some additional Y and Al which would be provided by the sialon phases. The α-sialon x value was slightly reduced during the M′ formation but remained unchanged after that, whereas the β-sialon z value showed a continuous decrease during heat treatment for up to 30 days, see Figs 6(a) and (b), respectively. The lower Al-O substitution level of the β' which formed during prolonged heat treatment and the constant Y-M′ content indicates that either the composition of the Y-M′ changed or that the liquid/glass became more cation-rich.

The phase changes of the Yb-doped α–β-sialon during heat treatment at 1450°C are shown in Fig. 5(b). An Yb-garnet phase formed in smaller amounts during the first 10 days, and the overall reaction pattern is similar to the Y-doped material.

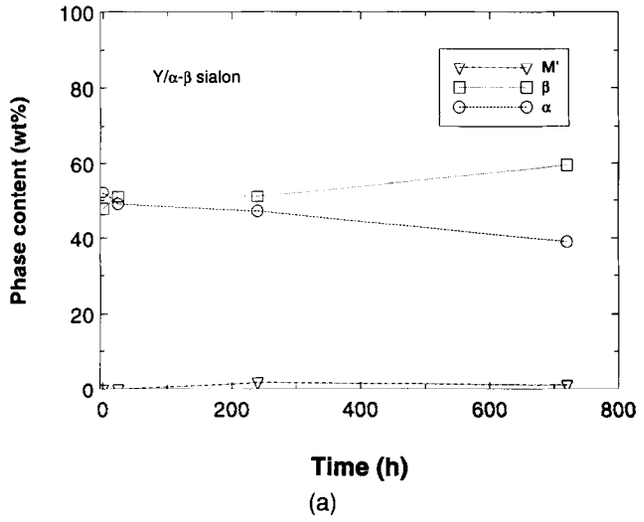

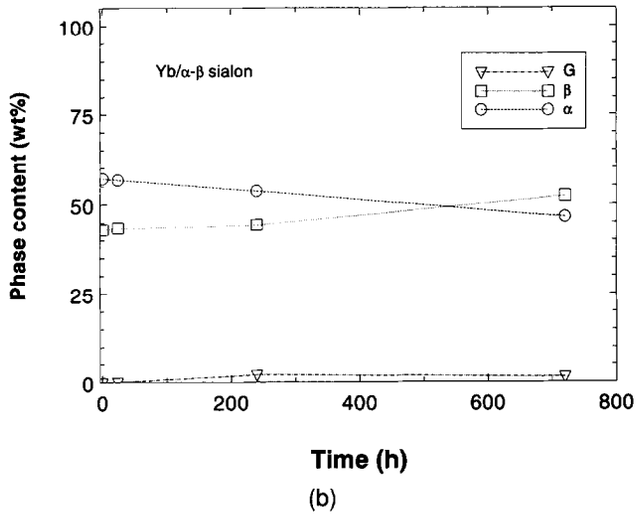

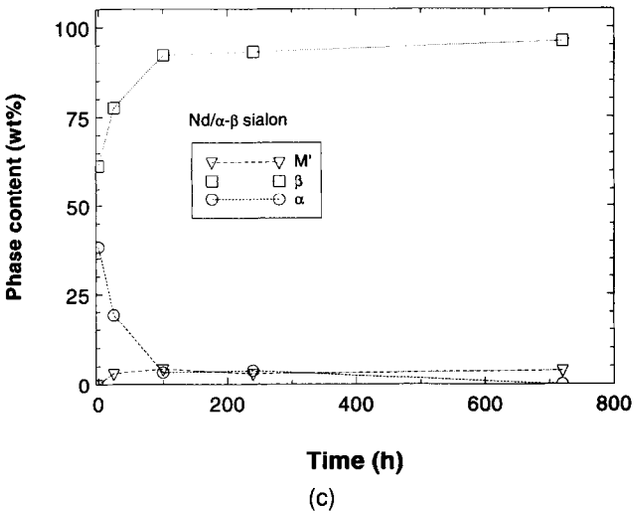

Fig. 5. The phase contents of the (a) Y-, (b) Yb- and (c) Nd-doped duplex sialons after heat treatment at 1450°C for extended periods of time. The sialons were fabricated from a starting powder composition corresponding to a $\beta'/\alpha'+\beta'$ weight ratio of 0·5.

However, the $\beta'/\alpha'+\beta'$ ratio did not change as much as in the Y-doped duplex sialon, and only smaller shifts between the two sialon phases were observed after 10 days. The substitution levels in the α' and β' structures determined by EDX in the TEM were in the same range as prior to heat treatment.

There was a pronounced transformation of α' to β', Al-substituted M′ and smaller amounts of the 21R sialon polytype in the Nd-doped duplex α–β-sialon during prolonged time of heat treatment at 1450°C, see Figs 5(c) and 7. α-Sialon could not be detected by XRD after 30 days at 1450°C. The z value of the β-sialon was initially shifted to a lower value when the major part of the α' phase decomposed, but was after that stabilized at a constant value, see Fig. 6(b).

The Nd-M′ phase, $Nd_2Si_{3-x}Al_xO_{3+x}N_{4-x}$, had x = 1·0 which represents the highest possible Al substitution in Nd-M′.[29,30] The Al content of the M′-phase was determined by comparison of the

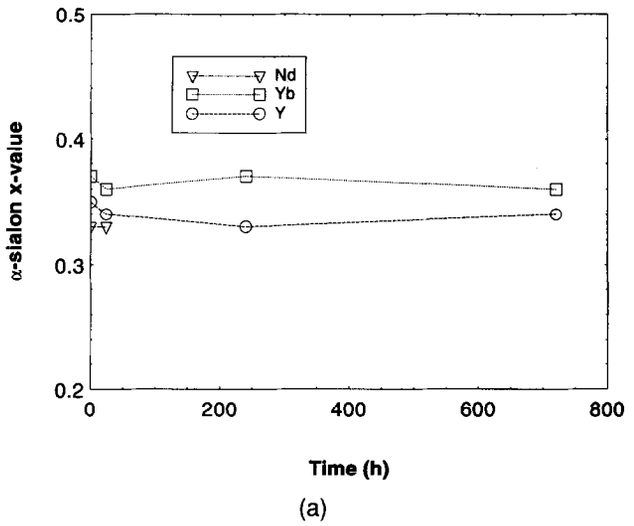

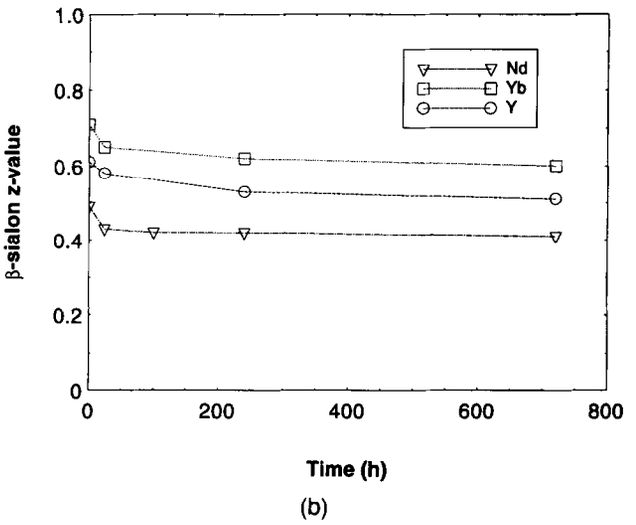

Fig. 6. (a) α-Sialon x value and (b) β-sialon z value after heat treatment at 1450°C for extended periods of time. The sialons were fabricated from a starting powder composition corresponding to a $\beta'/\alpha'+\beta'$ weight ratio of 0·5.

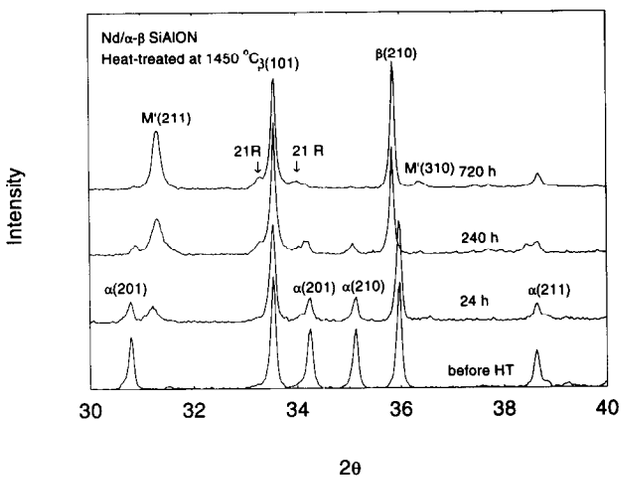

Fig. 7. Part of recorded X-ray diffractograms showing phase changes during heat treatment of the Nd-stabilized duplex sialon. Reflections from the 21R sialon polytype were observed after prolonged time at temperature. The Nd-stabilized sialon was fabricated from a starting powder composition corresponding to a $\beta'/\alpha'+\beta'$ weight ratio of 0·5.

tetragonal unit cell observed by XRD (a = 0·7758 nm and c = 0·5050 nm) with data on unit cell shift with composition (x value) given earlier.[29,30] This composition was also confirmed by EDX point analysis in the SEM. As expected, JEM phase, $NdAl(Si_{6-z}Al_z)(N_{10-z}O_z)$, was not observed after heat treatment at 1450°C; this phase forms predominantly at temperatures in the range 1550 to 1650°C.[15,21] The presence of the 21R sialon polytype was not easily determined in short-term heat-treated samples because of severe peak overlap. However, the increasing volume fraction with time at temperature could be established by comparison of XRD traces as illustrated in Fig. 7.

3.1.3 Reactions involving the α-sialon phase

The results from the heat treatments imply that the reactions involving the α-sialon phase are dependent on the α' stabilizing cation and, hence, the volume fraction and stability of secondary phases. Two, in principle, different reactions might take place; adjustment of the α' composition within the α-sialon phase field, and a decomposition of the α' into other phases.

The XRD results from the heat-treated duplex α–β microstructures formed with Y_2O_3 and Yb_2O_3 suggested that an adjustment of the α-sialon composition was the dominant reaction at 1450°C. This would provide elements required for the formation of the secondary crystalline phase (melilite and garnet in the case of Y and Yb, respectively). An adjustment of the α' composition within the two-dimensional phase field may take place according to the reaction:

$$\alpha'_1 + \text{liquid} \rightarrow \alpha'_2 + \text{M}' \text{ or garnet}$$

where α'_2 is an α sialon which has a lower x value than α'_1, i.e. the α-sialon composition moves towards the edge of the solid solution area. β-Sialon as well as N-rich phases like the 21R polytype may also form in this reaction.

When the α' composition has reached the edge of the α-sialon phase field, the amount of α-sialon may decrease through decomposition. This does not necessarily mean that the α'-phase is unstable in itself; the overall chemistry will determine the equilibrium phase composition. The presence of larger volumes of liquid/glass might contribute to an altered α'/β' ratio and a variation in the α- and β-sialon substitution levels at elevated temperatures.[10,11,31]

Sialons formed with Nd_2O_3 behaved in a significantly different way; the dominant reaction at temperatures around 1450°C seemed to be a decomposition of the Nd-stabilized α'-structure. The precipitation of Nd–M′ as well as the formation of β-sialon and the 21R sialon polytype continued during prolonged heat treatment. A decomposition of α-sialon with the assistance of a liquid phase might take place in the following way:

$$\alpha' + \text{liquid} \rightarrow \beta' + \text{M}' + 21\text{R}$$

It cannot be excluded that the α'-phase might decompose directly without the aid of a liquid. However, solid state reactions would be extremely slow due to the poor self-diffusivity in these sialon structures.

The high-temperature behaviour of the duplex α–β-sialons formed with Nd_2O_3 was similar to that of Sm-doped α–β-sialons.[24] Both Sm^{3+} and Nd^{3+} have fairly large cation sizes, 0·096 nm and 0·099 nm, respectively, which might, indirectly, contribute to the observed instability of the α'-structure. It has been shown that larger rare earth cations form very stable melilite phases with extended Al substitution.[29,30] Thus, there is a 'competition' between the α sialon and the R–M′ phase for the rare earth element and nitrogen at temperatures around 1450°C.

3.2 General microstructures

3.2.1 As-sintered sialon ceramics

SEM of carefully polished cross-sections showed that all compositions reached full density during hot-pressing. The microstructures of the duplex α–β-sialons consisted of a large number of needle-shaped β' grains in an α-sialon matrix. The general microstructures of the duplex α–β-sialons fabricated from starting powder mixtures with compositions corresponding to $\beta'/\alpha'+\beta'$ weight ratios of 0·3 and 0·5 are shown in Fig. 8 for the three different oxide additives. The dark areas in

these images are the β-sialon grains and the lighter grey areas the α-sialon matrix. The images suggest that the choice of rare earth metal oxide affects the β-sialon grain size distribution. The liquid phase sintering medium that formed when Nd_2O_3 was added seemed to promote β' grain growth, while the addition of Yb_2O_3 resulted in a more finely dispersed β' phase. The β' grain size in the α-β-sialons fabricated with Y_2O_3 was slightly coarser than in the duplex sialons fabricated with Yb_2O_3, see Fig. 8.

The bright contrasts in the SEM images in Fig. 8 represent the intergranular regions, and it can be seen that only smaller volume fractions of secondary phases are present in the microstructures. The intergranular volume fraction seemed to be further reduced when the $\beta'/\alpha'+\beta'$ weight ratio aimed at by the starting powder composition was increased from 0·3 to 0·5. This may be explained by the presence of two sialon phases with extended solid solutions and the resulting ability to locally accommodate smaller variations in chemistry.

A number of the α' grains in the duplex sialons showed the type of core/shell structure which has previously been observed in α and duplex α-β-sialons stabilized by Dy and Sm,[14,24] see Fig. 9. The cores were shown by electron diffraction and EDX to be either pure α-Si_3N_4 or β', while the

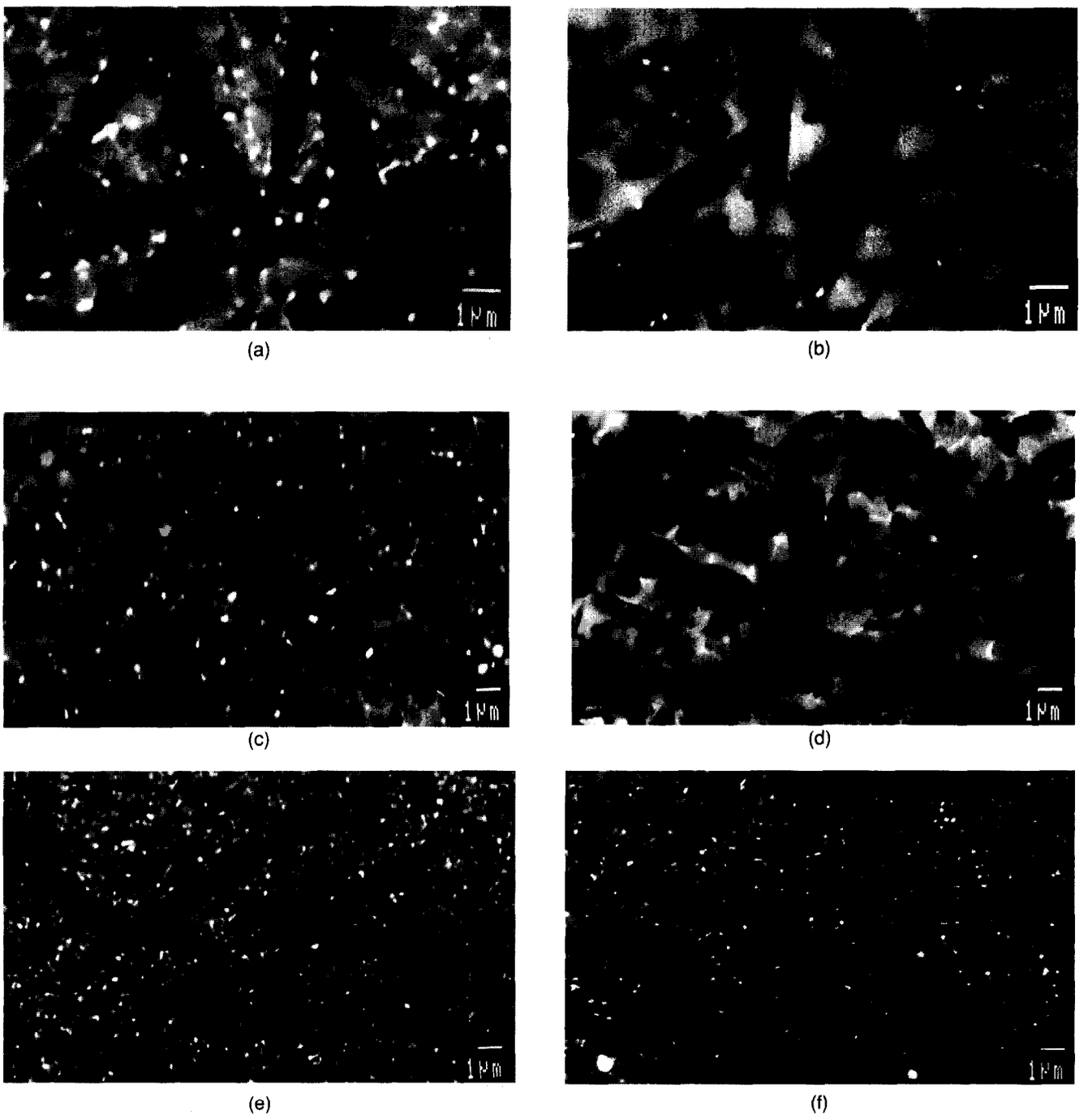

Fig. 8. The general microstructures of duplex sialons stabilized by Nd, Y or Yb fabricated from starting powder compositions corresponding to $\beta'/\alpha'+\beta'$ weight ratios of 0·3 and 0·5. (a) Nd, 0·3; (b) Nd, 0·5; (c) Y, 0·3; (d) Y, 0·5; (e) Yb, 0·3; (f) Yb, 0·5.

shells always contained the α' stabilizing cation. This shows that α', in addition to homogeneous nucleation in a supersaturated liquid, may nucleate and grow on only partially dissolved α-Si_3N_4 particles from the starting powder mixture as well as on β' nuclei.

3.2.2 Heat-treated sialon ceramics

The extensive transformation of α' to β' and M′ during heat treatment of the Nd-stabilized duplex sialon at 1450°C was clearly revealed in the SEM, Fig. 10(a). The initially prismatic β' grain morphology could not be distinguished after 10 days at the heat-treatment temperature. The microstructures of the duplex sialons fabricated with Y_2O_3 and Yb_2O_3 underwent coarsening during heat treatment, see Figs 8 and 10. Elongated β' grains were, however, still present after 10 days at 1450°C. The limited M′ and garnet formation in these microstructures at 1450°C was clearly demonstrated also in the SEM, Fig. 10.

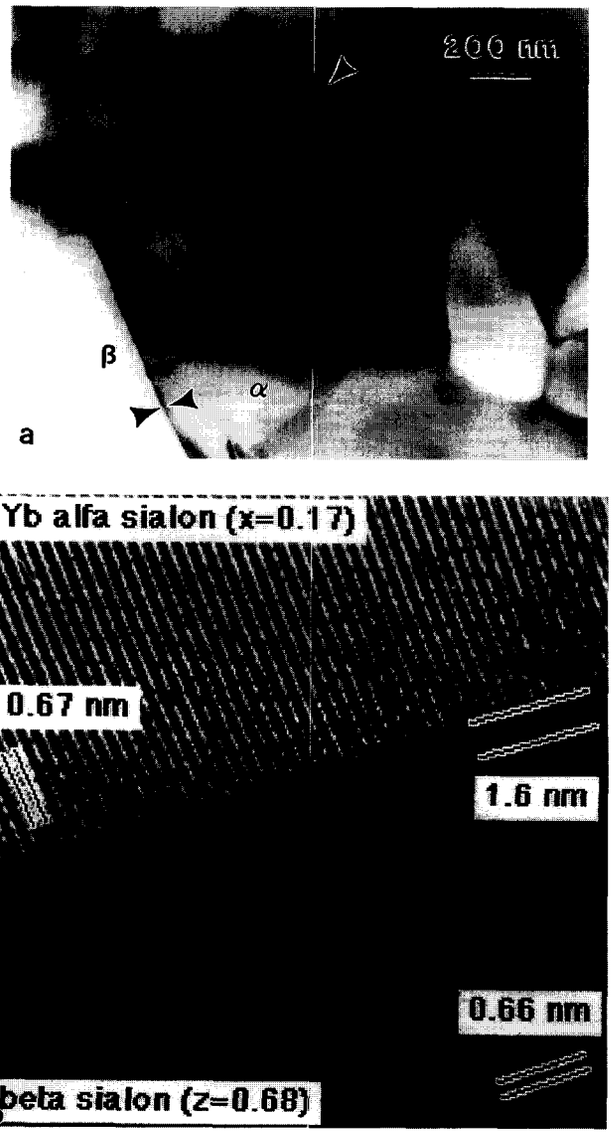

Fig. 9. (a) α-Sialon grain (arrowed) with a core/shell structure in the Yb-stabilized duplex sialon formed with a starting powder composition corresponding to a $\beta'/\alpha'+\beta'$ weight ratio of 0·5. (b) High resolution TEM image of the α/β-sialon grain boundary marked in (a) indicating a film thickness of around 1·6 nm.

3.3 Intergranular microstructure of duplex α–β-sialons

3.3.1 As-sintered Yb and Nd sialon ceramics

The microstructures of the Yb and Nd duplex α–β-sialons formed with a starting powder mixture

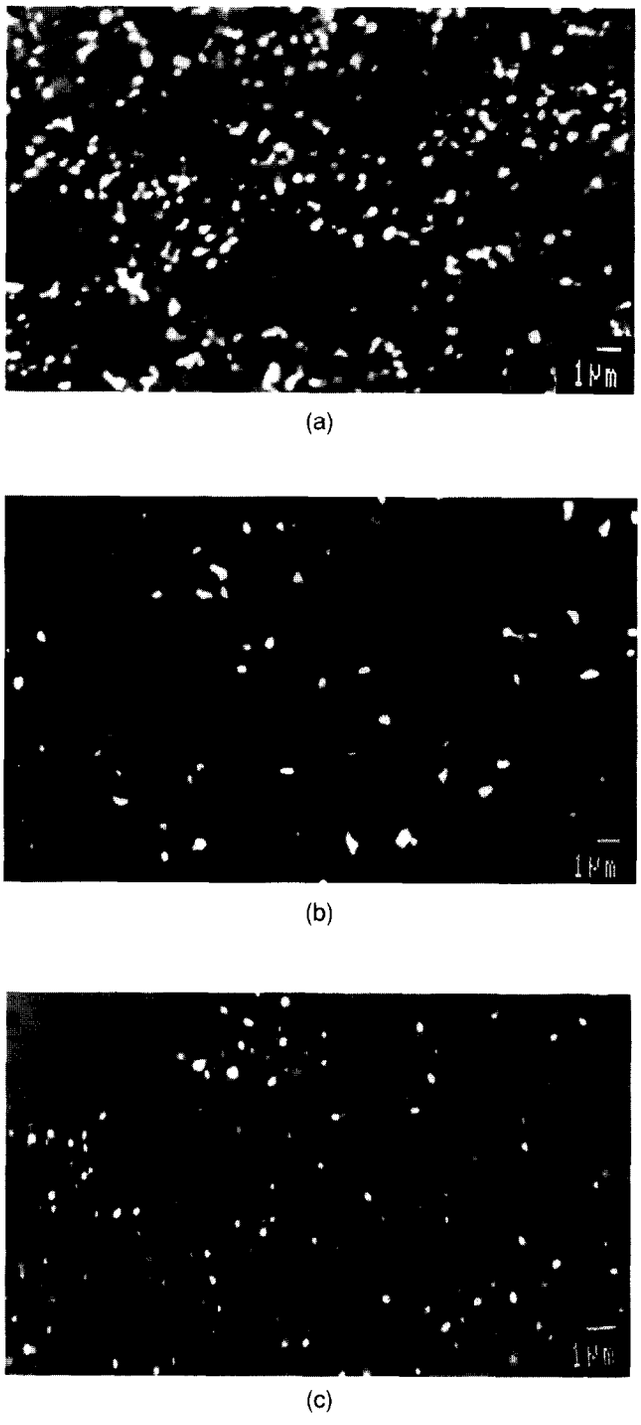

Fig. 10. The general microstructures of duplex sialons stabilized by (a) Nd, (b) Y and (c) Yb after heat treatment at 1450°C for 10 days. The sialons were fabricated from a starting powder composition corresponding to a $\beta'/\alpha'+\beta'$ weight ratio of 0·5.

corresponding to an $\beta'/\alpha'+\beta'$ weight ratio of 0·5, contained a continuous intergranular network of residual glass. The thickness of the amorphous grain boundary films was in the range 1·5 to 2·5 nm, and the films were rich in Al and the α' stabilizing cation, see Figs 9 and 11–14.

The grain boundary films merged into glassy pockets at multi-grain junctions in the duplex Nd-stabilized sialon, Figs 12 and 13. The composition of these pockets seemed to be dependent upon the

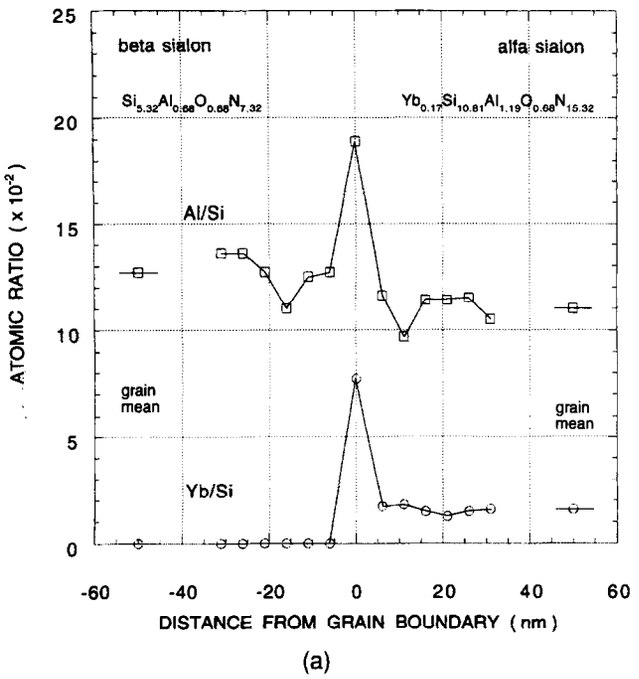

Fig. 11. EDX concentration profiles across α'/β' grain boundaries in the (a) Yb- and (b) Nd-stabilized duplex sialons formed with a starting powder composition corresponding to a $\beta'/\alpha'+\beta'$ weight ratio of 0·5. High resolution TEM images of the boundaries are shown in Figs 9(b) and 13, respectively.

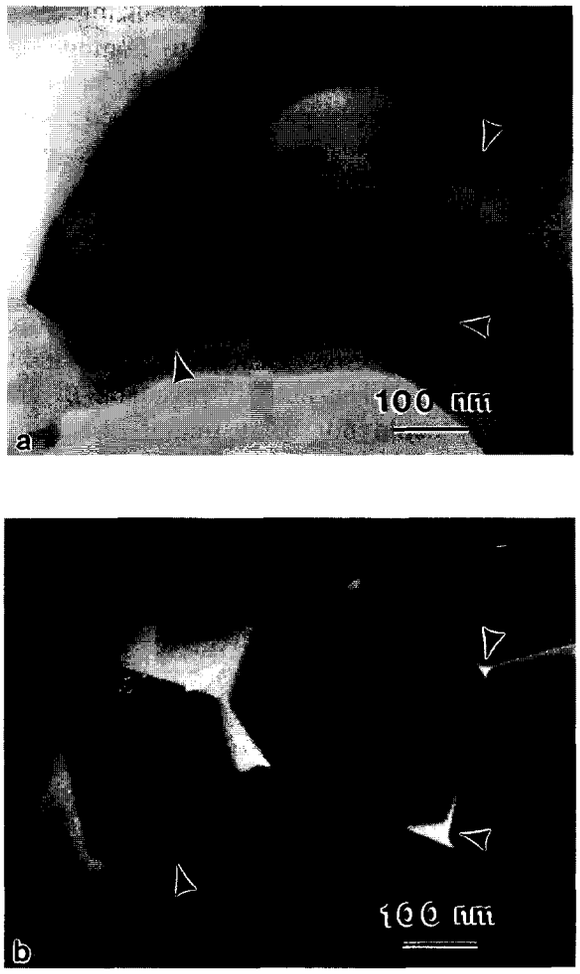

Fig. 12. The continuous intergranular glassy phase (arrowed) in the Nd-stabilized duplex sialon formed with a starting powder composition corresponding to a $\beta'/\alpha'+\beta'$ weight ratio of 0·5. (a) TEM bright field image. (b) TEM centred dark field image formed from diffuse scattered electrons.

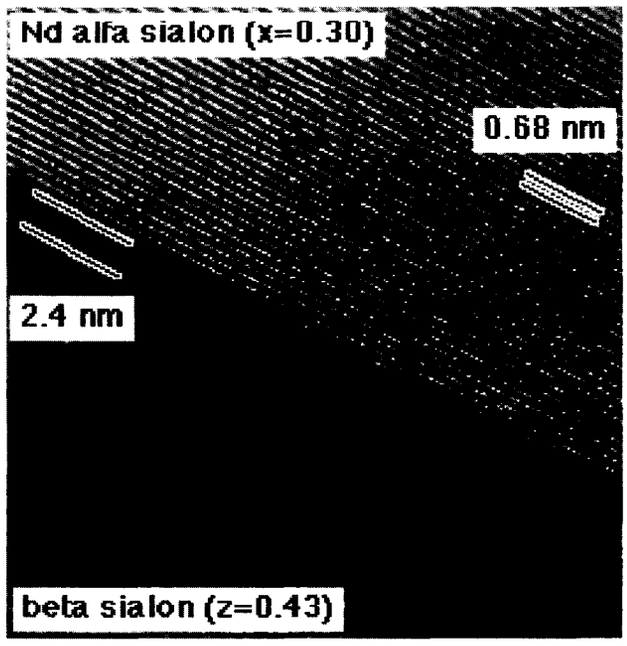

Fig. 13. High resolution TEM image of an α'/β' boundary indicating a film thickness of 2·4 nm in the Nd-stabilized duplex sialon formed with a starting powder composition corresponding to a $\beta'/\alpha'+\beta'$ weight ratio of 0·5.

structure and substitution level of the adjacent sialon grains; glassy pockets surrounded by β' grains had a significantly higher Nd/Si cation ratio than pockets facing α' grains. The Al/Si cation ratio of the glass could not be correlated to the structure of the surrounding sialon grains.

Also extremely small (≤ 5 nm) pockets at multi-grain junctions in the Yb-stabilized duplex sialon contained a secondary crystalline phase, Fig. 14. Full crystallization of the pockets had, however, not been obtained; thin glassy films separated the Yb-, Al- and Si-rich crystalline phase from adjacent sialon grains. The volume fraction of this secondary crystalline phase was obviously too low for detection by XRD, and a complete structure determination has not yet been carried out. However, EDX analysis in the FEGTEM showed cation compositions close to that of B-phase, R_2SiAlO_5N. B-phases are stable at small rare earth cation radii, and form at temperatures in the range 950 to 1100°C.[32] This suggests that the crystalline intergranular phase present in the microstructure of the duplex sialon stabilized by Yb formed through crystallization of glass pockets during cooling from the densification temperature.

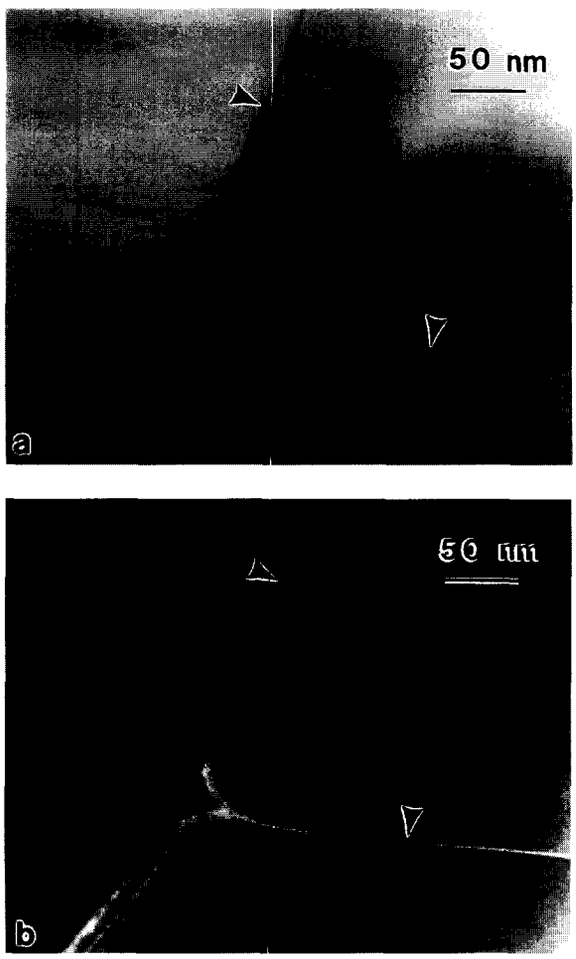

Fig. 14. Pocket containing a crystalline Yb-, Al- and Si-rich phase separated from surrounding sialon grains by thin films of residual glass in the duplex Yb-sialon formed with a starting powder composition corresponding to a $\beta'/\alpha'+\beta'$ weight ratio of 0·5. Glassy films (arrowed) were present also at sialon grain boundaries. (a) TEM bright field image. (b) TEM centred dark field image formed from diffuse scattered electrons.

The size of the pockets at multi-grain junctions varied within the microstructures, but there was no obvious size difference between the Nd- and Yb-stabilized duplex sialons.

3.3.2 Heat-treated Yb α–β sialon

The secondary crystalline phase in the Yb-stabilized duplex sialon with an $\beta'/\alpha'+\beta'$ weight ratio of around 0·5 was present as smaller grains after heat treatment at 1450°C, see Fig. 15. The Yb/Al atomic ratios of the analysed grains were close to that of the Yb, Al-garnet, $3Yb_2O_3{\cdot}5Al_2O_3$, which is consistent with the XRD results. This implies that the secondary crystalline phase present in the as-sintered material had been dissolved, and that the intergranular liquid present at 1450°C provided an effective diffusion path and thereby enabled grain growth of the secondary crystalline phase. Thin intergranular films of residual glass were present throughout the microstructure also after heat treatment. Formation of glassy pockets at multi-grain junctions was, however, not observed, see Fig. 15.

3.4 Mechanical properties

Vickers hardness (HV_{10}) and indentation fracture toughness (K_{IC}) of the α and duplex α–β-sialons are summarized in Fig. 16. It can be seen that the presence of β-sialon in an α-sialon matrix resulted in a good combination of mechanical properties when the starting powder mixture had a composition corresponding to a $\beta'/\alpha'+\beta'$ weight ratio of 0·5.

The hardness showed only minor changes with increasing β-sialon contents up to around 50 wt%, while higher β-sialon contents caused a gradual decrease in hardness. This reflects the lower hardness of the β-sialon which is around 17 GPa. The highest indentation fracture toughness was obtained when Yb_2O_3 was used as the stabilizing oxide in a duplex α–β-sialon with an $\beta'/\alpha'+\beta'$ weight ratio of around 0·4, see Fig. 16(b).

The results thus imply that the optimum combination of structure and properties is obtained with an $\beta'/\alpha'+\beta'$ weight ratio of around 0·5. These duplex α-β sialon ceramics would have a high hardness (HV_{10} around 21 GPa) and a high toughness (K_{IC} around 5–5·5 MPa $m^{1/2}$). This is similar to some observations on previously characterized duplex sialons.[14,22–24]

The mechanical properties of the duplex α–β-sialons after heat treatment at 1450°C are summarized in Fig. 17. The hardness of the Nd-doped

duplex sialon was significantly reduced during the first 10 days of heat treatment while the Y- and Yb-doped sialons showed only a smaller reduction in hardness after the early stages of heat treatment. The observed effect of heat treatment upon hardness could be predicted from the phase contents shown in Fig. 5. The measured hardness is dependent upon the volume fractions and hardness of the constituent phases; the presence of α' (which has a hardness of around 22 GPa) contributes to a high hardness.[4] The Nd-doped duplex sialon transformed into β-sialon and Nd–M′ with

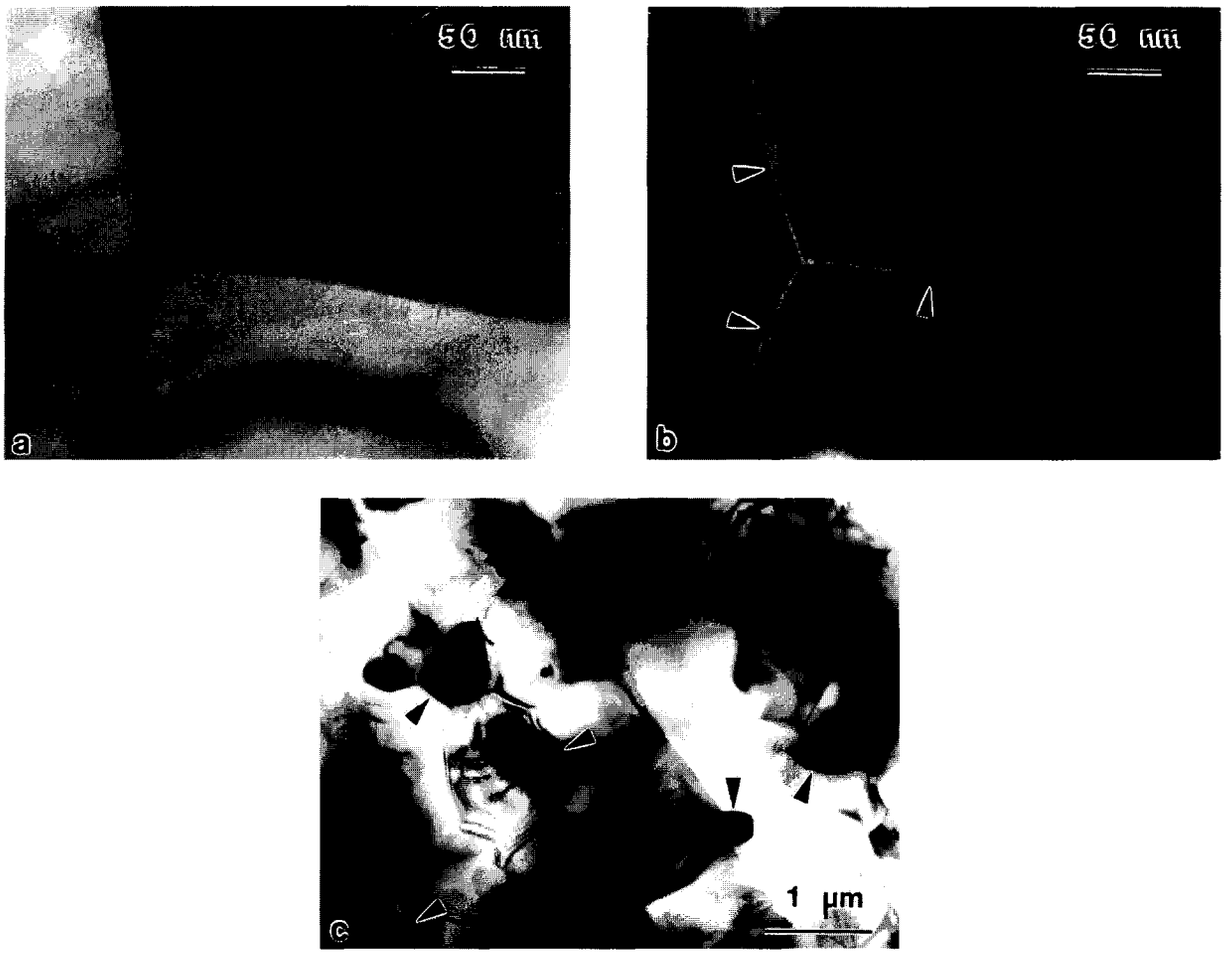

Fig. 15. The intergranular microstructure of the duplex Yb-sialon formed with a starting powder composition corresponding to a $\beta'/\alpha'+\beta'$ weight ratio of 0·5 after heat treatment at 1450°C. Thin intergranular films of residual glass, arrowed in (b), were present throughout the microstructure. (a) TEM bright field image and (b) centred dark field image formed from diffuse scattered electrons. Grains of Yb, Al-garnet are arrowed in (c).

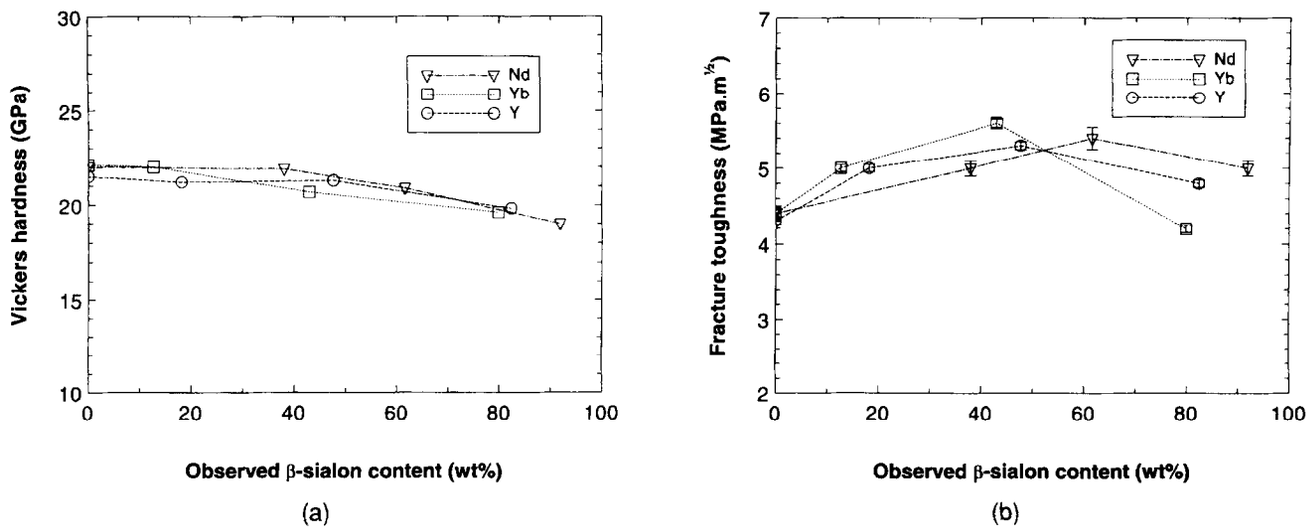

Fig. 16. (a) Vickers hardness (HV_{10}) and (b) indentation fracture toughness (K_{IC}) as functions of observed β-sialon content.

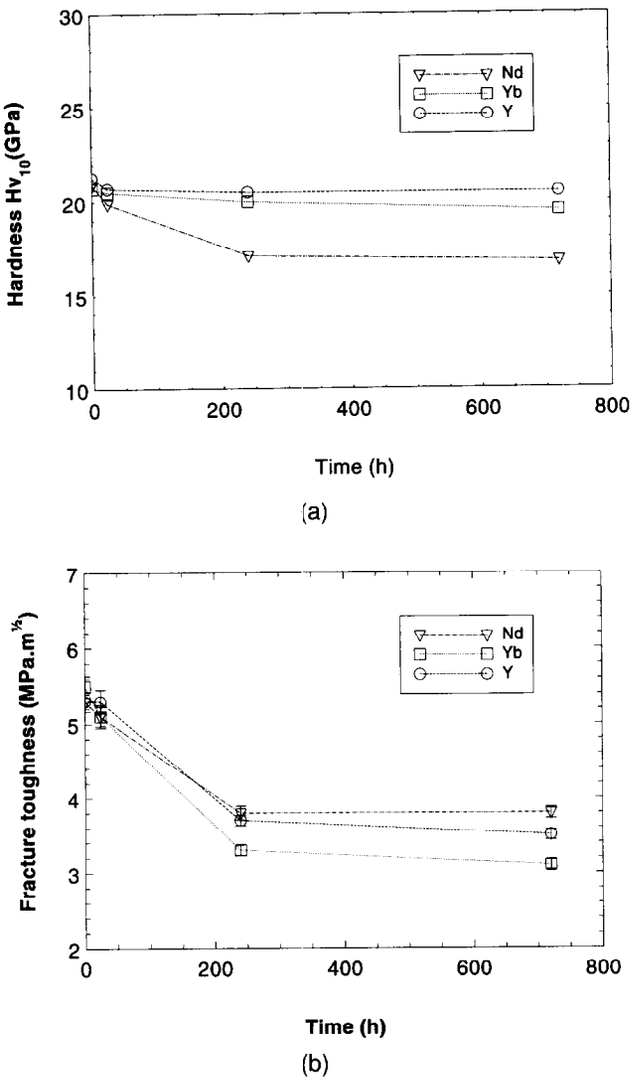

Fig. 17. (a) Vickers hardness (HV_{10}) and (b) indentation fracture toughness (K_{IC}) as function of observed β-sialon content after heat treatment at 1450°C for extended periods of time. The sialons were fabricated from a starting powder composition corresponding to a $\beta'/\alpha'+\beta'$ weight ratio of 0·5.

time at 1450°C which accounts for the observed reduction in hardness.

The indentation fracture toughness was strongly reduced after heat treatment for 10 days, also for the Y- and Yb-stabilized duplex sialons, see Fig. 17. This could possibly be explained by the altered β-sialon morphology; the initially fibrous microstructure would promote high fracture toughness. Prolonged heat treatment at 1450°C did not cause any significant further reduction in toughness.

4 Conclusions

1. Dense, duplex α–β-sialon ceramics with only smaller volume fractions of intergranular phases can be prepared using Y or the rare earth elements Yb and Nd as the α' stabilizing element.
2. The microstructure of the intergranular regions is dependent upon the α-sialon stabilizing element.
3. The $\beta'/\alpha'+\beta'$ weight ratio as well as the α- and β-sialon substitution levels are dependent upon the α' stabilizing element.
4. Y and Yb gives an α-sialon phase which is stable during long-term heat treatment at 1450°C. Nd gives a less stable α-sialon resulting in the formation of melilite, $Nd_2Si_{3-x}Al_xO_{3+x}N_{4-x}$ (x = 1), β-sialon and the 21R sialon polytype during prolonged heat treatment at 1450°C.
5. Duplex α–β-sialon ceramics with an $\beta'/\alpha'+\beta'$ weight ratio of around 0·5 have high room temperature hardness (HV_{10} around 21 GPa) and indentation fracture toughness (5·0–5·5 MPa $m^{1/2}$).
6. Y or Yb as the stabilizing element in the duplex α–β-sialons seem to be good choices, but Yb_2O_3 is, however, considerably more expensive than Y_2O_3. Nd_2O_3 does not give a duplex microstructure that is stable at high temperatures.

Acknowledgements

Zhi-Jian Shen acknowledges the Swedish Institute for a scholarship during the time when this work was carried out. Economic support of this project was received from the Swedish Research Council for Engineering Sciences.

References

1. Jack, K. H., Review: Sialons and related nitrogen ceramics. *J. Mater. Sci.*, 1976, **11**, 1135–1158.
2. Lewis, M. H., Leng-Ward, G. and Jasper, C., Sintering additive chemistry in controlling microstructure and properties of nitrogen ceramics. *Ceram. Powder Sci.*, 1988, **2**, 1019–1033.
3. Ekström, T. and Nygren, M., Sialon ceramics. *J. Am. Ceram. Soc.*, 1992, **75**, 259–276.
4. Ekström, T., Hardness of dense Si_3N_4-based ceramics. *J. Hard. Mater.*, 1993, **4**, 77–95.
5. Cao, G. Z. and Metselaar, R., α-Sialon ceramics: A review. *Chem. Mater.*, 1991, **3**, 242–252.
6. Hampshire, S., Park, H. K., Thompson, D. P. and Jack, K. H., α-Sialon ceramics. *Nature (Lond.)*, 1978, **274**, 880–882.
7. Jack, K. H., Silicon nitride, sialons, and related ceramics. In *Ceramics and Civilization, Vol. III, High-Technology Ceramics.* American Ceramic Society, Columbus, OH, 1986, pp. 259–288.
8. Sun, W. Y., Tien, T. Y. and Yen, T.-S., Solubility limits of α-sialon solid solutions in the system Si, Al, Y/N, O. *J. Am. Ceram. Soc.*, 1991, **74**, 2547–2550.
9. Stutz, D., Greil, P. and Petzow, G., Two-dimensional solid-solution forming of Y-containing α-Si_3N_4. *J. Mater. Sci. Lett.*, 1986, **5**, 335–336.

10. Mandal, H., Thompson, D. P. and Ekström, T., Reversible α–β-sialon transformation in heat-treated sialon ceramics. *J. Eur. Ceram. Soc.*, 1993, **12**, 421–429.
11. Ekström, T. and Shen, Z.-J., Temperature stability of rare earth doped α-sialon ceramics. In *5th Intern. Symp. on Ceramic Materials and Components for Engines*, ed. D. S. Yan, X. R. Fu and S. X. Shi. World Sci. Publ. Co., 1995, pp. 206–210.
12. Cheng, Y. B. and Thompson, D. P., Preparation and grain boundary devitrification of samarium α-sialon ceramics. *J. Eur. Ceram. Soc.*, 1994, **14**, 13–21.
13. Shen, Z.-J., Ekström, T. and Nygren, M., Temperature stability of samarium doped α-sialon ceramics. *J. Eur. Ceram. Soc.* 1996, **16**, 43–53.
14. Falk, L. K. L., Shen, Z.-J. and Ekström, T., α–β-Sialon ceramics in the Dy–Si–Al–O–N and Sm–Si–Al–O–N systems. In *Fourth Euro Ceramics*, Vol. 2, ed. C. Galassi. Gruppo Edit. Faenza Editrice, Italy, 1995, pp. 163–168.
15. Shen, Z.-J., Ekström, T. and Nygren, M., Homogeneity region and thermal stability of neodymium doped α-sialon ceramics. *J. Am. Ceram. Soc.*, 1996, **79**, 721–732.
16. Shen, Z.-J., Ekström, T. and Nygren, M., Ytterbium as a stabiliser of α-sialon ceramics. *J. Appl. Phys. D*, in press.
17. Shen, Z.-J., Ekström, T. and Nygren, M., Preparation and properties of stable dysprosium doped α-sialon ceramics. *J. Mater. Sci.*, in press.
18. Mandal, H. and Thompson, D. P., Mechanism for α-β transformation. In *Fourth Euro Ceramics*, Vol. 2, ed. C. Galassi. Gruppo Ed. Faenza Editrice, Italy, 1995, pp. 327–334.
19. Mandal, H. and Thompson, D. P., Effect of type of rare earth oxide additive on the design of sialon ceramics. In *Fourth Euro Ceramics*, Vol. 2, edit. C. Galassi. Gruppo Edit. Faenza Editrice, Italy, 1955, pp. 273–280.
20. Cheng, Y.-B., Mandal, H. and Thompson, D. P., Post-sintering heat treatment of rare earth α-sialon ceramics. In *Fourth Euro Ceramics*, Vol. 2, ed. C. Galassi. Gruppo Edit. Faenza Editrice, Italy, 1995, pp. 341–346.
21. Grins, J., Shen, Z.-J., Nygren, M. and Ekström, T., Preparation and crystal structure of $LaAl(Si_{6-z}Al_z)N_{10-z}O_z$. *J. Materials. Chem.*, 1995, **5**, 2001–2006.
22. Ekström, T., Effect of composition, phase content and microstructure on the performance of yttrium SiAlON ceramics. *Mater. Sci. Eng.*, 1989, **A109**, 341–349.
23. Sheu, T.-S., Microstructure and mechanical properties of the in-situ β-Si_3N_4/α-SiAlON composite. *J. Am. Ceram. Soc.*, 1994, **77**, 2345–2353.
24. Ekström, T., Falk, L. K. L. and Shen, Z.-J., Duplex α–β-sialon ceramics stabilized by dysprosium and samarium. *J. Am. Ceram. Soc.*, in press.
25. Johansson, K.-E., Palm, T. and Werner, P.-E., An automatic microdensitometer for X-ray powder diffraction photographs. *J. Phys.*, 1980, **E13**, 1289–1291.
26. Ekström, T., Käll, P.-O., Nygren, M. and Olsson, P.-O., Single-phase β-sialon ceramics by glass-encapsulated hot isostatic pressing. *J. Mater. Sci.*, 1989, **24**, 1853–1861.
27. Käll, P.-O., Quantitative phase analysis of Si_3N_4-based materials. *Chem. Scripta*, 1988, **28**, 439–446.
28. Anstis, G. R., Chantikul, P., Lawn, B. R. and Marshall, D. B., A critical evaluation of indentation techniques for measuring fracture toughness. *J. Am. Ceram. Soc.*, 1981, **64**, 533–538.
29. Cheng, Y.-B. and Thompson, D. P., Aluminium-containing nitrogen melilite phase. *J. Am. Ceram. Soc.*, 1994, **77**, 143–148.
30. Wang, P.-L., Tu, H. Y., Sun, W. Y., Yan, D. S., Nygren, M. and Ekström, T., On the solid solubility of Al in the melilite systems $R_2Si_{3-x}Al_xO_{3+x}N_{4-x}$ with R = Nd, Sm, Gd, Dy, Yb and Y. *J. Eur. Ceram. Soc.*, 1995, **15**, 689–695.
31. Shen, Z.-J., Ekström, T. and Nygren, M., Reactions occurring in post-heat treated α–β-sialons; On the thermal stability of a-sialon ceramics. *J. Eur. Ceram. Soc.*, in press.
32. Thompson, D. P., New grain-boundary phases for nitrogen ceramics. In *Mat. Res. Soc. Symp. Proc.* Vol. 287, ed. I.-W. Chen, P. F. Becker, M. Mitomo, G. Petzow and T.-S. Yen. Materials Research Society, Pittsburgh, Pennsylvania, 1993, pp. 79–92.